

Silver Nanoparticles Textured Oxide Thin Films for Surface Plasmon Enhanced Photovoltaic Properties

Amitabha Nath

NIT Agartala: National Institute of Technology Agartala

Naveen Bhati

NIT Agartala: National Institute of Technology Agartala

Bikram Kishore Mahajan

Purdue University School of Electrical and Computer Engineering

Jayanta Kumar Rakshit

NIT Agartala: National Institute of Technology Agartala

Mitra Barun Sarkar (✉ mbarun.ece@nita.ac.in)

National Institute of Technology Agartala <https://orcid.org/0000-0002-4590-7955>

Research Article

Keywords: Thin Films, Ag nanoparticles, Localized surface plasmon resonance, Photovoltaic properties.

Posted Date: May 19th, 2021

DOI: <https://doi.org/10.21203/rs.3.rs-495274/v1>

License:  This work is licensed under a Creative Commons Attribution 4.0 International License.

[Read Full License](#)

Version of Record: A version of this preprint was published at Plasmonics on August 3rd, 2021. See the published version at <https://doi.org/10.1007/s11468-021-01509-3>.

Silver Nanoparticles Textured Oxide Thin Films for Surface Plasmon Enhanced Photovoltaic Properties

Amitabha Nath¹, Naveen Bhati^{1,2,4,5}, Bikram Kishore Mahajan³, Jayanta Kumar Rakshit^{1,4}, and Mitra Barun Sarkar^{1,*}

¹*Department of Electronics and Communication Engineering, National Institute of Technology Agartala, Jirania-799046, INDIA*

²*Department of Electrical Engineering, National Institute of Technology Agartala, Jirania-799046, INDIA*

³*School of Electrical and Computer Engineering, Purdue University, West Lafayette, IN 47907 USA*

⁴*Department of Electronics and Instrumentation Engineering, National Institute of Technology Agartala, Jirania-799046, INDIA*

⁵*Department of Electrical Engineering, Indian Institute of Technology Roorkee, Uttarakhand-247667, INDIA*

***corresponding author: Name:** Mitra Barun Sarkar, **Email:** mbarun.ece@nita.ac.in

Abstract:

In this report, Ag nanoparticles were fabricated using single-step glancing angle deposition (SS-GLAD) technique upon In₂O₃/TiO₂ thin film. Afterwards, a detailed analysis was done for the two samples such as In₂O₃/TiO₂ thin film and In₂O₃/TiO₂ thin film/Ag nanoparticles, to inspect the field emission scanning electron microscopy (FESEM), X-ray diffraction (XRD), ultraviolet (UV) spectroscopy and electrical properties. The reduction in bandgap energy for the samples of In₂O₃/TiO₂ thin film/Ag nanoparticles (~4.16 eV) in comparison with the In₂O₃/TiO₂ thin film (~4.28 eV) was due to trapped *e-h* recombination at the oxygen vacancies and electron transmission of Ag to the conduction band of the In₂O₃/TiO₂ thin films. Moreover, under irradiation of photons Ag nanoparticles generated inorganic Ag-O compound attributable to the localized surface plasmon resonance (LSPR). Also, a ~90% high transmittance, ~60% and ~25% low reflectance in UV and visible region, fill factor (FF) of 53%, as well as power conversion efficiency (PCE) of 15.12% was observed for In₂O₃/TiO₂ thin film/Ag nanoparticles than the In₂O₃/TiO₂ thin film. Therefore, the use of Ag nanoparticles textured In₂O₃/TiO₂ thin film based device is a promising approach for the forthcoming photovoltaic applications.

Keywords:

Thin Films, Ag nanoparticles, Localized surface plasmon resonance, Photovoltaic properties.

1. INTRODUCTION:

With the growing world population, one of the greatest challenges our society is currently facing is that of clean energy. Solar energy, being abundant, presents itself as a lucrative solution and this led researchers all over the world in pursuit of various photovoltaic devices, which can convert sunlight to electrical energy for numerous applications. While

the commercial solar panels are still predominantly manufactured from crystalline Silicon, researchers are exploring various materials, configurations, and fabrication techniques to develop highly efficient, inexpensive, and reliable photovoltaic devices. Among them dye sensitized solar cells [1-3], perovskites [4, 5], quantum-dots [6-8], organic material based solar cells [9-10] etc., has been explored by various research groups around the world in last couple of decades.

One of the major objectives of the solar cell researchers in any material or configuration is to achieve high absorption of photons, which can lead to high efficiency. To circumvent the limits posed by the 'diffusion length' of the charge carriers, researchers sometimes incorporate back side reflectors or attempt to 'trap' the photons inside device, which leads to increased photon path length or optical thickness. The later approach can be achieved by texturing the surface which can guide the scattered light within the active material, leading to longer photon path length and hence improved efficiency. A popular technique of texturing the surface is by depositing various shapes and sizes of metal nanoparticles. One of the first reports in this area was by Stuart *et. al* [11], where silver nanoparticles deposited on silicon-on-insulator (SOI) photodetector enhanced the photocurrent by an order of magnitude. This was achieved due to a phenomenon known as localized surface plasmon resonance (LSPR). LSPR is induced when the frequency of the incoming photon matches with that of the oscillating electrons of the nanoparticle, leading to an increased electromagnetic field which aids in light concentration around the nanoparticle. This phenomenon of guided light, coupled with strong light scattering due to the nanoparticles, has led to tremendous research interest in recent years and several nanoparticles *viz.*, gold (Au) [12-14], silver (Ag) [15-17], aluminium (Al) [18-20] etc., nanorods [21-23], nano discs [24, 25], has been explored, leading to high efficiency.

In addition to classical solar cells based on p-n junction, novel structures such as photoelectrochemical solar cells [26], and solar cells based non schottky diodes [27], metal-insulator-semiconductor (MIS) solar cells [28], semiconductor-insulator-semiconductor (SIS) solar cells [29], etc., has been explored by various research groups around the world. Among them SIS structures showed enormous potential as low-cost photovoltaic devices. In SIS structures, instead of a p-n junction, the separation of charges are carried out by the electric field at the semiconductor-insulator interface. Several SIS structures (*e.g.*, ITO/SiO_x/p-Si, Al-SiO_x/p-Si, etc.) has been fabricated and analysed since 1980s [29]. Combining the SIS structures with LSPR presents a lucrative approach to fabricate low-cost, high efficiency solar cells. In addition, one can also tailor the photovoltaic device to absorb the desired wavelengths in the solar spectrum, for specific applications. This can be achieved by a suitable choice of active materials to construct a multi-junction solar cell. Titanium dioxide (TiO₂) ($E_g \sim 3.2$ eV) and Indium oxide (In₂O₃) ($E_g \sim 3.6$ eV) are some of the most extensively used materials due to their availability, ease of handling, low cost, non-toxicity and its optoelectronic applications [30, 31]. By itself TiO₂ shows the properties of photovoltaic devices [8, 24] however by the incident of photons and incorporation of In₂O₃ with TiO₂, the nanostructures boost up the photoexcited *e-h* pairs due to several scattering processes, which lead to increase the device efficiency. Here, we have reported an efficient photovoltaic device for UV region by depositing Ag nanoparticles on the top of TiO₂ and In₂O₃ thin films, where the Ag nanoparticles enhanced the quantum efficiency of the device by coupling incident light into guided modes through LSPR effect. The device is fabricated using SS-GLAD technique, without the requirement of any annealing step which makes the device inexpensive, thereby making the device attractive for potential commercialization.

2. EXPERIMENTAL:

2.1 Synthesis of $\text{In}_2\text{O}_3/\text{TiO}_2$ Thin Film

ITO coated glass substrate (99.999% pure, MTI Corporation, USA) were cleaned using methanol, acetone and deionized water. For further cleaning, the substrates were dipped into a mixed solution of hydrofluoric acid and deionized water with a dilution ratio of 1:50. A dense thin film (~ 100 nm) of TiO_2 has been synthesized upon pre-cleaned ITO coated glass substrate using electron beam evaporator (e-beam) (HHV Co. (p) Ltd., Model-15F6) with a base pressure of 0.05 mbar. A high vacuum chamber pressure of $\sim 0.2 \times 10^{-4}$ mbar and deposition rate of 1.2×10^{-10} m/s was maintained during the synthesis of TiO_2 thin film. The thin film substrate holder was held at a perpendicular distance of ~ 16 cm from the evaporated material source. Similar technique has been followed to synthesize the In_2O_3 thin film (~ 100 nm) over the TiO_2 thin film at a deposition rate of 0.5×10^{-10} m/s.

2.2 Fabrication of Ag Nanoparticles

SS-GLAD technique has been carried out to fabricate the Ag (highly pure 99.999%) nanoparticles over $\text{In}_2\text{O}_3/\text{TiO}_2$ thin film. The crucible filled with Ag pellets was placed at a vertical distance of < 30 cm from the substrate holder with an azimuthal angle and a spin of 85° and 460 rpm respectively. A deposition rate of 1.2×10^{-10} m/s was maintained during the fabrication of Ag nanoparticles, as well.

2.3 Device Fabrication

To fabricate the device, Indium (In) (99.999% pure beads, MTI Corporation, USA) has been deposited on the samples through an aluminium mask hole (each hole diameter: $\sim 1.95 \times 10^{-6}$ m²), which act as the electrode for the device. Here two distinct devices, viz., $\text{In}_2\text{O}_3/\text{TiO}_2$ thin film and $\text{In}_2\text{O}_3/\text{TiO}_2$ thin film/Ag nanoparticles, were fabricated, as shown in Figure 1(a) and (b) respectively.

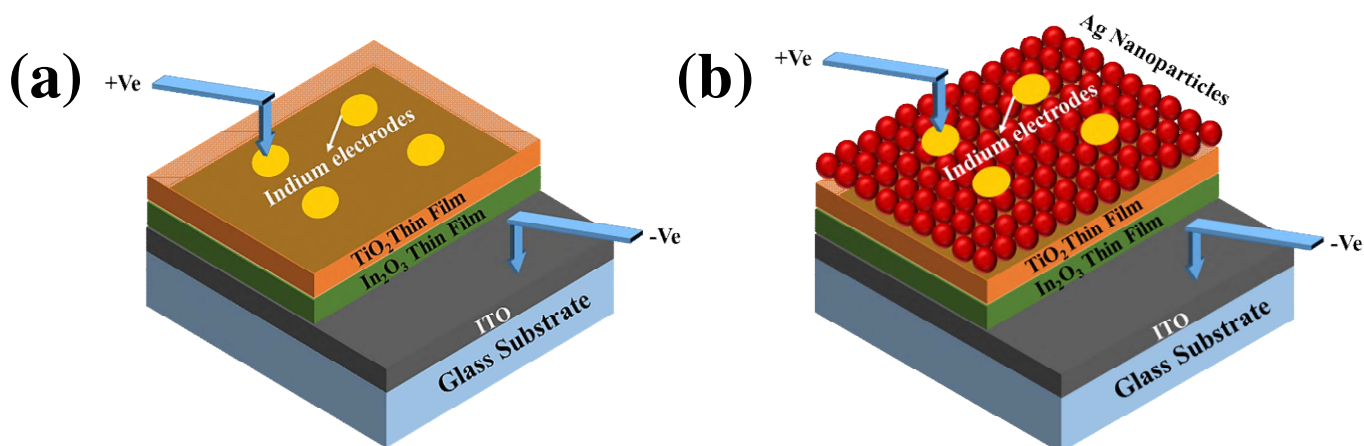


Fig. 1 Schematic diagram of the fabricated devices: (a) $\text{In}_2\text{O}_3/\text{TiO}_2$ thin film, (b) $\text{In}_2\text{O}_3/\text{TiO}_2$ thin film/Ag nanoparticles.

2.4 Characterizations

FESEM and energy dispersive x-ray analysis (EDAX) has been done to morphologically characterize the samples using SIGMA-300 (Zeiss). The XRD were done on a Bruker D8 Advance diffractometer to study the structural characterization. The absorption, reflection and transmission spectrum were recorded by a Perkin Elmer LAMBDA 950 UV-VIS-NIR Spectrophotometer. The electrical characteristics were investigated using a Keysight B2902A source and measurement units (SMU).

3. RESULTS AND DISCUSSIONS:

3.1 Morphological Analysis of Fabricated Structures

The morphology of the fabricated thin film and nanoparticles were shown in Figure 3(a) and (b). Figure 3(b) shows the FESEM image of the $\text{In}_2\text{O}_3/\text{TiO}_2$ thin film/Ag nanoparticles sample using SS-GLAD technique, where the Ag nanoparticles were densely packed and randomly distributed all over the thin film surface. The growth of densely packed nanoparticles was aided by high substrate temperature in the vacuum chamber [31]. This technique is preferred here because of its highly user-friendly interface and easily controllable features (rotation speed, azimuthal angle, evaporation rate, substrate temperature etc.) [32]. The particle size histogram (Fig. 3(c)) shows that the Ag nanoparticles range between ~4 nm to ~40 nm, and a huge percentage of the deposited particles had diameter between ~7 nm to ~12 nm. Figure 3(d) shows the EDAX spectra of $\text{In}_2\text{O}_3/\text{TiO}_2$ thin film/Ag nanoparticles sample, where elemental composition of oxygen (O [K]), tin (Sn [L]), silver (Ag [L]), indium (In [L]), and titanium (Ti [K]) was detected. Table-I listed the atomic and weight percentage of elements present in the sample.

Table-I: EDAX data

Element	Weight (%)	Atomic (%)	Kratio
O K	3.40	15.53	0.0042
Sn L	9.61	25.01	0.0659
Ag L	55.19	37.40	0.5226
In L	29.78	18.96	0.2568
Ti K	2.02	3.09	0.0160
Total	100.00		

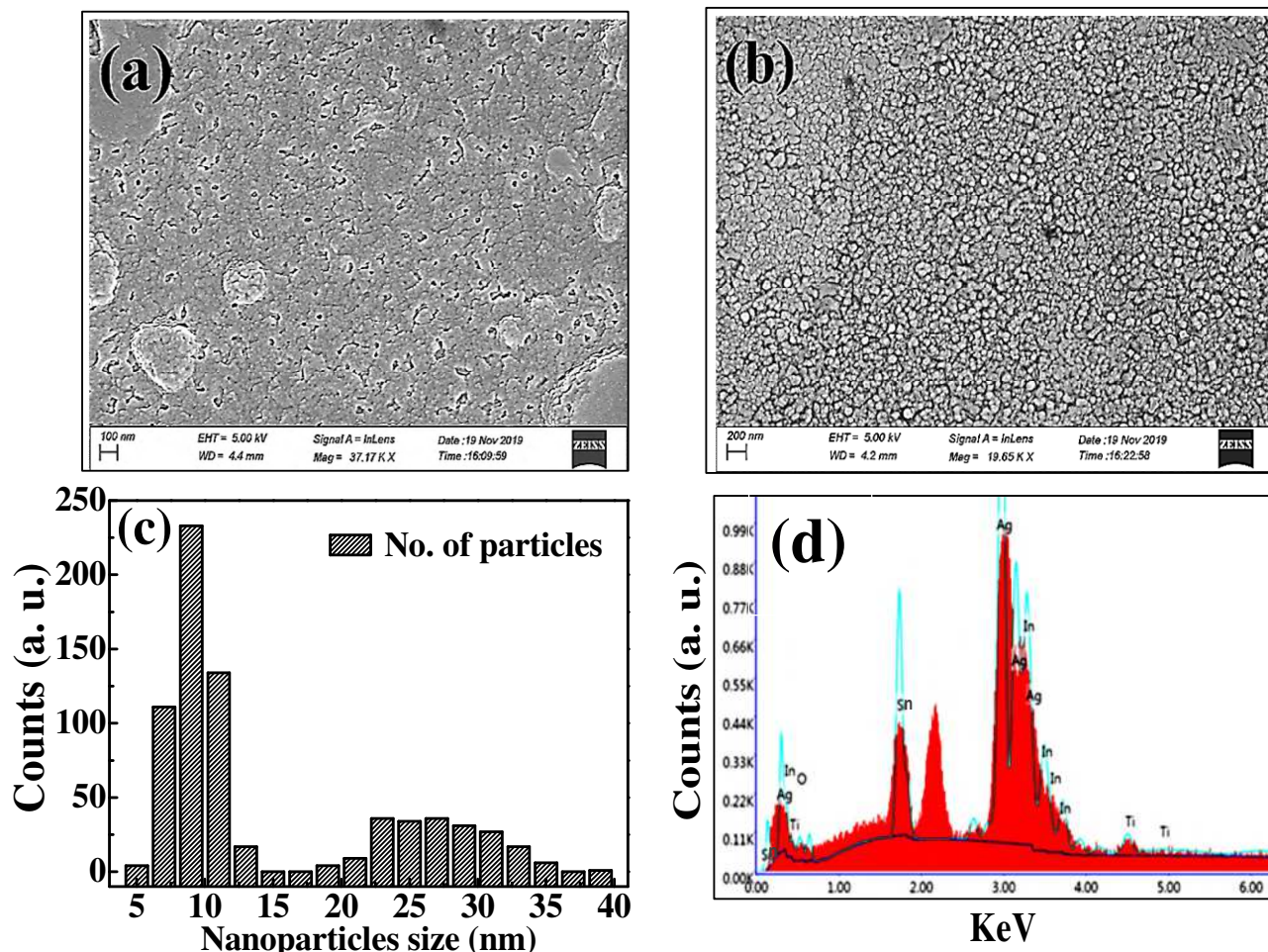


Fig. 2 Top view FESEM images of (a) In₂O₃/TiO₂ thin film, (b) In₂O₃/TiO₂ thin film/Ag nanoparticles, (c) Particle size histogram image of Ag nanoparticles, (d) EDAX analysis of the sample.

3.2 Structural analysis:

More information about the phases, crystal orientations, and morphology of the In₂O₃/TiO₂ thin film and In₂O₃/TiO₂ thin film/Ag nanoparticles samples can be analysed from XRD measurements, carried out using Bruker D8 Advanced using Cu-K α target source under the diffraction angle (2θ) between 20° to 80°. Figure 3(a) shows the XRD peaks for In₂O₃/TiO₂ thin film. The peaks (211), (222), (431) corresponds to In₂O₃ (JCPDS card no. 06–0416) [33] and the peaks (103), (200), (220), (125) corresponds to TiO₂ anatase phase (JCPDS card no. 89–4921) [34]. The planes of (111), (200), (220), and (311) corresponds to Ag peaks (JCPDS card no. 03-0921) [34] which were formed due to the deposition of Ag nanoparticles over the In₂O₃/TiO₂ thin film. Additionally, the peaks (031) and (242) corresponds to Ag₃O₄ monoclinic crystal structure (JCPDS card no. 84-1261) which is attributed to the formation of Ag-O compound [27, 30] during fabrication. W. Xie *et al.* [35], Dhar Dwivedi *et al.* [34], A. Laskri *et al.* [36] also reported such type of Ag-O compound during the synthesis of Ag nanoparticles. Therefore, the XRD patterns confirms the presence of In₂O₃, TiO₂ and Ag in the fabricated samples.

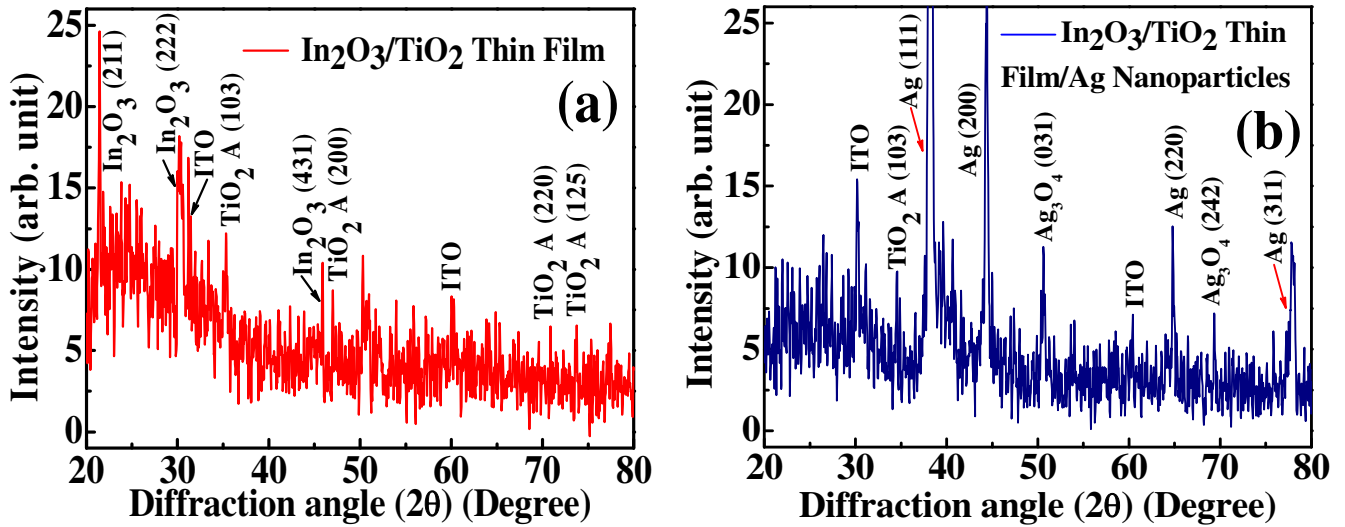


Fig. 3 XRD profiles for (a) In₂O₃/TiO₂ thin film (b) In₂O₃/TiO₂ thin film/Ag nanoparticles.

3.3 Optical properties analysis:

Figure 4(a) shows the comparison of absorption spectra of In₂O₃/TiO₂ thin film with In₂O₃/TiO₂ thin film/Ag nanoparticles on ITO coated glass substrate in the wavelength range of 200–800 nm. A ~45 nm red shift has been observed in the UV region for In₂O₃/TiO₂ thin film/Ag nanoparticles sample which may be the effect of localized surface plasmon resonance of Ag nanoparticles in the later sample [37]. Under irradiation, the Ag nanoparticles exhibit a large electron oscillation and generated inorganic Ag-O compound, as previously explained in the structural analysis section. This inorganic Ag-O compound was generated due to localized surface plasmon and thus absorption of light in the UV region has been occurred. Figure 4(b) compares the measured reflectance of both samples using UV-Vis diffused reflectance spectroscopy (DRS), where In₂O₃/TiO₂ thin film/Ag nanoparticles exhibits a significantly lower reflectivity in the UV (~60%) and visible (~25%) region after applying only Ag nanoparticles on the seed layer (thin film). This dropping of reflectance can be an indication of the reduction of bandgap energy for the In₂O₃/TiO₂ thin film/Ag nanoparticles. To demonstrate the bandgap energy of the samples Kubelka-Munk function method [38]. According to the theory of P. Kubelka and F. Munk, the diffusive reflectance can be written as,

$$[F(R)] = \frac{K}{S} = \frac{(1-R)^2}{2R} \dots \dots \dots (1)$$

where, ‘R’ is the measured reflectance, ‘K’ is the molar absorption coefficient, ‘S’ is the scattering factor, ‘h’ is the Planck’s constant, and [F(R)] is known as the Kubelka-Munk function. In the plot, the linear extrapolation over the ‘hv’ axis of (F(R)hv)² versus hv gives the values of bandgap, where the bandgap energy of ~4.28 eV and ~4.16 eV was obtained and demonstrated in Figure 4(c) for In₂O₃/TiO₂ thin film and In₂O₃/TiO₂ thin film/Ag nanoparticles respectively. The reduction in bandgap energy is accredited to the red shift of Ag nanoparticles coated sample which is due to the trapped e-h recombination at the oxygen vacancies and electron transmission of Ag to the conduction band of the oxide thin films [39]. The optical transmittance spectra in Figure 4(d), shows a ~90% transmittance in the UV region, for the In₂O₃/TiO₂ thin film/Ag nanoparticles as compared to ~50% of that of the In₂O₃/TiO₂ thin film. Hence, it proves that the light falls on the Ag nanoparticles surface completely gets transmitted by reducing the amount of reflection loss.

Moreover, the presence of oxygen vacancies leads to add the additional energy levels in the bandgap, known as Urbach tail. The Urbach tails of the samples were characterized from the Urbach energy (E_U) (Eq. 2) plot with the incident photon energy.

$$\ln(\alpha) = \ln(\alpha_0) + \left(\frac{h\nu}{E_U}\right) \dots\dots\dots(2)$$

Where, α is known as absorption coefficient, α_0 is a constant, $h\nu$ is incident photon energy, and E_U is the Urbach energy [40, 41]. The E_U signifies the spread of defect energy states inside the bandgap. The E_U was also used to analyse the sample performance, since the E_U affects the carrier mobility, carrier lifetime, and cell performance [42]. The reciprocal of the slope value of the linear portion of $\ln(\alpha)$ versus $h\nu$ shown in Fig. 4(e) was utilized to estimate E_U value. The calculated value of E_U was 3.45 eV and 4.90 eV for the $\text{In}_2\text{O}_3/\text{TiO}_2$ thin film and $\text{In}_2\text{O}_3/\text{TiO}_2$ thin film/Ag nanoparticles samples respectively. This enhancement in E_U was due to the presence of oxygen vacancies in the Ag nanoparticles decorated sample [43], which corroborates the previous UV analysis.

Figure 4(f) depicts the variation of light harvesting efficiency (LHE) for $\text{In}_2\text{O}_3/\text{TiO}_2$ thin film with $\text{In}_2\text{O}_3/\text{TiO}_2$ thin film/Ag nanoparticles samples between the wavelength ranges of 350–800 nm. Here, the enhanced LHE characteristics for $\text{In}_2\text{O}_3/\text{TiO}_2$ thin film/Ag nanoparticles samples suggests the enhanced light absorption due to the incorporation of Ag nanoparticles on the thin film samples [44]. According to the Beer-Lambert law, the LHE characteristics can be further enhanced by increasing the length of the optical path by modifying the nanocrystalline films [45]. The LHE characteristics can be obtained using Eq. 3.

$$\text{LHE}(\lambda) = 1 - 10^{-\alpha d} \dots\dots\dots(3)$$

Where α and d is the absorption coefficient and thickness of the nanocrystalline film [44].

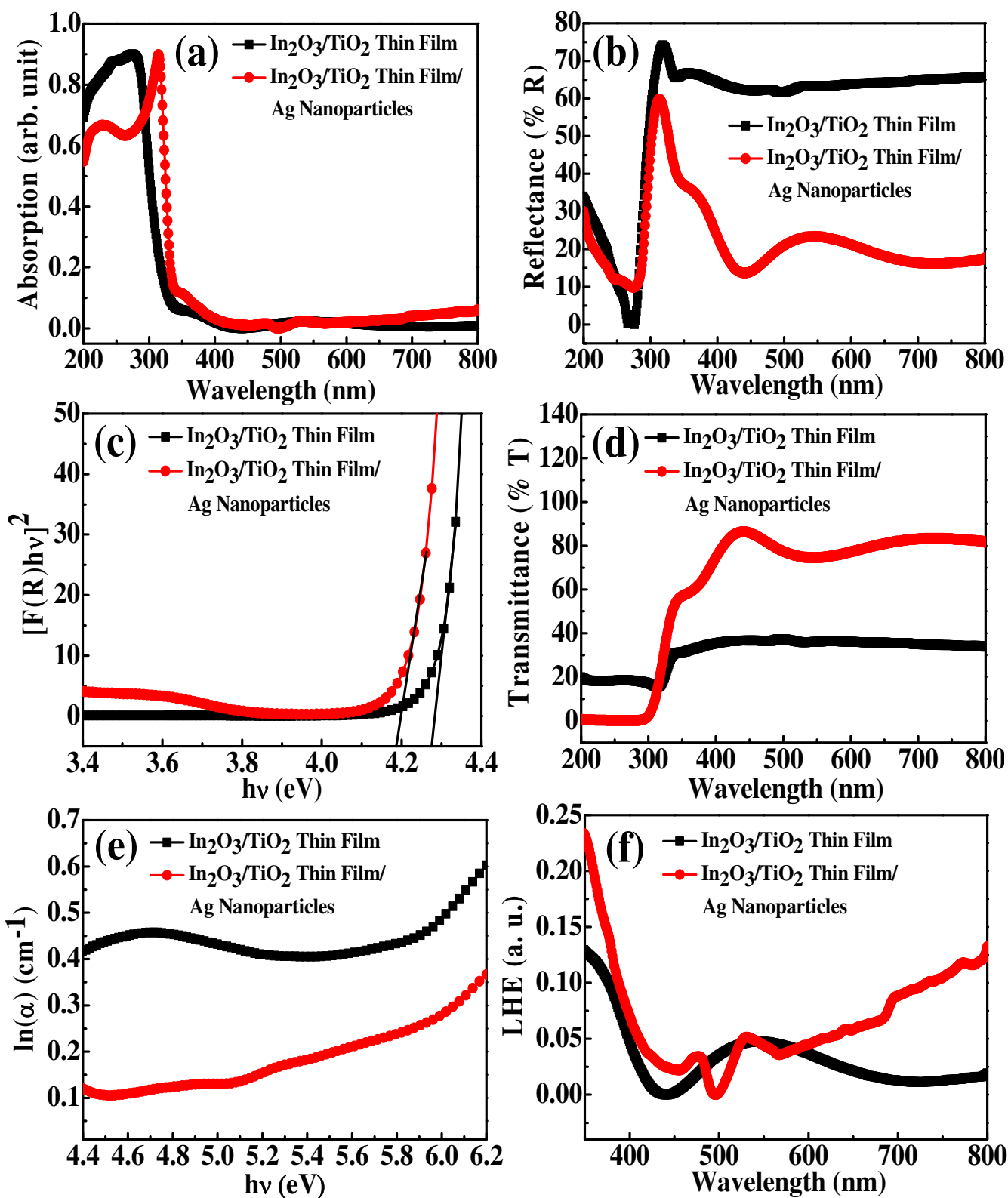


Fig. 4 (a) Absorption spectra, (b) UV-DRS spectra (reflectance spectra), (c) Kubelka-Munk plot (for bandgap), (d) Transmittance spectra, (e) Urbach energy, (f) Light harvesting efficiency (LHE) characteristics of $\text{In}_2\text{O}_3/\text{TiO}_2$ thin film and $\text{In}_2\text{O}_3/\text{TiO}_2$ thin film/Ag nanoparticles samples on a ITO coated glass substrate.

3.5 Analysis of electrical characteristics:

The power conversion efficiency (η) of the $\text{In}_2\text{O}_3/\text{TiO}_2$ thin film/Ag nanoparticles device and the $\text{In}_2\text{O}_3/\text{TiO}_2$ thin film device need to be characterised. For this purpose, the photovoltaic parameters, namely open circuit voltage (V_{OC}), short circuit photocurrent density (J_{SC}), and fill factor (FF) were obtained. Figure 5(a) shows the experimental setup for the measurement of photovoltaic parameters, where a tungsten filament source is illuminating the fabricated devices at room temperature. A B2902A source and measurement unit (SMU) has been used for recording the characteristics. The obtained J - V curve for $\text{In}_2\text{O}_3/\text{TiO}_2$ thin film and $\text{In}_2\text{O}_3/\text{TiO}_2$ thin film/Ag nanoparticles devices, were plotted in Figure 5(b). Table-II lists the corresponding measured photovoltaic parameters considering an effective device area of 1.8 mm^2 for both the devices.

It has been found that the maximum current that the device can deliver *i.e.*, the short circuit photocurrent density (J_{SC}), or the current that flows in the circuit when the electrodes are shorted, was enhanced by $\sim 136\%$ for the $\text{In}_2\text{O}_3/\text{TiO}_2$ thin film/Ag nanoparticles device compared to that of the $\text{In}_2\text{O}_3/\text{TiO}_2$ thin film. The maximum voltage delivered by the device or open circuit voltage (V_{OC}), also increases for the $\text{In}_2\text{O}_3/\text{TiO}_2$ thin film/Ag nanoparticles device. The fill factor (FF) which is the ratio between the maximum power of the device and the product of V_{OC} and J_{SC} has been found to be 58% and 53% for the $\text{In}_2\text{O}_3/\text{TiO}_2$ thin film/Ag nanoparticles device and the $\text{In}_2\text{O}_3/\text{TiO}_2$ thin film device respectively. All these parameters leads to an increase of ~ 127 times enhancement in the power conversion efficiency (η) for the $\text{In}_2\text{O}_3/\text{TiO}_2$ thin film/Ag nanoparticles device (15.12%) compared to the $\text{In}_2\text{O}_3/\text{TiO}_2$ thin film device (11.90%). This significant enhancement in efficiency is attributed due to the LSPR effect, introduced by the depositing plasmonic Ag nanoparticles [44].

Table II. Photovoltaic parameters for the two device structures.

Device Structure	V_{OC} (Volt)	J_{sc} ($\mu\text{A}/\text{cm}^2$)	FF (%)	η (%)
ITO/ $\text{In}_2\text{O}_3/\text{TiO}_2$ thin film	0.88	22.9	58	11.90
ITO/ $\text{In}_2\text{O}_3/\text{TiO}_2$ thin film/Ag nanoparticles	0.91	31.1	53	15.12

The overall PCE (η) was estimated at room temperature from the short circuit photocurrent density (J_{SC}), open circuit voltage (V_{OC}), and the fill factor of the sample (FF) to the power of the incident light (P_{light}), as given by the Eq. 4 [46].

$$\%PCE (\eta) = \frac{(J_{sc} V_{oc} FF)}{P_{light}} \dots\dots\dots(4)$$

Where, the FF was determined from the ratio of maximum power (P_{max}) of the samples per unit area to the V_{OC} and J_{SC} [46].

$$FF = \frac{P_{max}}{(V_{oc} J_{sc})} \dots\dots\dots(5)$$

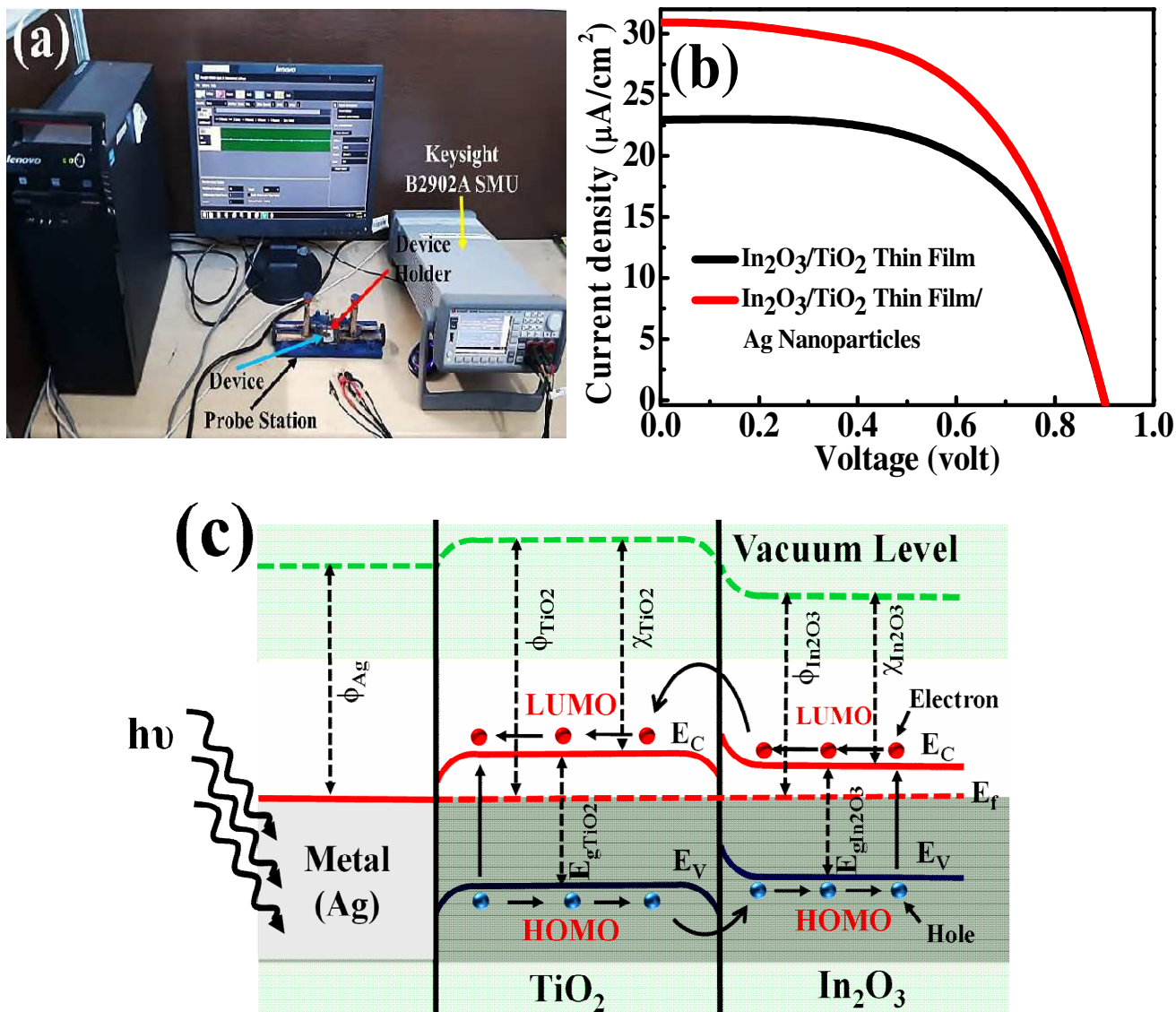


Fig. 5 (a) Experimental setup for the measurement of photovoltaic parameters, (b) J - V curve for $\text{In}_2\text{O}_3/\text{TiO}_2$ thin film and $\text{In}_2\text{O}_3/\text{TiO}_2$ thin film/Ag nanoparticles devices, (c) A schematic illustration of the staggered gap diagram.

Figure 5(c) shows the staggered gap diagram of the $\text{In}_2\text{O}_3/\text{TiO}_2$ thin film/Ag nanoparticles device, where Φ and χ is the work function and electron affinity of Ag NPs, TiO_2 and In_2O_3 respectively. When the light ($h\nu$) is illuminated on the device, electrons are excited state from the highest occupied molecular orbital (HOMO) to the lowest unoccupied molecular orbital (LUMO) [46], which are then collected. The Ag nanoparticles increases the photon path which leads to higher conversion efficiencies. Table-III depicts the comparison of state-of-the-art of this work with other reported work based on the device performances. Therefore, a low cost SS-GLAD technique of fabricating high efficiency solar cells which are aided by the LSPR effect of the deposited Ag nanoparticles has been studied. The fabrication step doesn't require further processing steps after SS-GLAD which makes the device inexpensive, thereby making the device attractive for potential commercialization.

Table III. Comparison of state-of-the-art of this work with other reported work.

Sl. No.	Device name	FF (%)	η (%)	References
1	Ag NPs textured In ₂ O ₃ /TiO ₂ thin films	53	15.12	[This work]
2	TiO ₂ photoelectrode morphology of N719 DSSC	74.1	9.8	[47]
3	In ₂ O ₃ /CdS/CuInS ₂ thin-film solar cell	61	9.7	[48]
4	n-AZO nanorod solar cell	39.38	6.25	[49]
5	Dye sensitized nanocrystalline TiO ₂ solar cell	63	5.6	[50]
6	nb-doped TiO ₂ /Sn-doped In ₂ O ₃ multi-layered DSSC	70.9	5.13	[51]
7	Mn dopant in CdS quantum dot sensitized solar cell	55	3.29	[52]
8	Nanoporous TiO ₂ film based DSSC	60	2.87	[53]
9	SnO ₂ photoanode treated with TiCl ₄	57	2.85	[54]
10	ZnO nanoparticles based dye-sensitized solar cells	48.5	1.97	[55]

4. Conclusion:

Here, a thorough analysis were done for In₂O₃/TiO₂ thin film and In₂O₃/TiO₂ thin film/Ag nanoparticles samples to inspect the morphological, structural and optical characteristics. The marginal optical bandgap energy (~4.16 eV), high transmittance (~90%), low reflectance in UV (~60%) and visible (~25%) region, Jsc of 31.1 mA/cm², Voc of 0.91 volt, FF of 53%, and PCE of 15.12% was observed for In₂O₃/TiO₂ thin film/Ag nanoparticles as compared to the In₂O₃/TiO₂ thin film. Therefore, the use of Ag nanoparticles textured oxide thin film based device is a promising approach for the photovoltaic applications.

Acknowledgements: The authors are acknowledged to Central Instrumentation Centre, Tripura University, INDIA for providing FESEM and EDAX facility. The authors also thankful to Dr. B. Saha, Assistant Professor, Department of Physics, NIT Agartala, INDIA for providing the XRD and optical measurement facility.

Funding: Not Applicable.

Conflict of Interest: The authors declare that they have no conflict of interest.

Availability of data and material: The materials described in the manuscript, including all relevant raw data, will be freely available from the corresponding author upon reasonable request.

Code availability: Not Applicable.

Authors' Contribution:

Amitabha Nath: Methodology, Device fabrication, Electrical measurements, Data analysis, Writing – original draft.

Naveen Bhati: Characterizations and data analysis.

Bikram Kishore Mahajan: Analysis, Writing and editing.

Jayanta Kumar Rakshit: Validation and editing.

Mitra Barun Sarkar: Conceptualization, Validation, Editing and Supervision.

Declarations:

Ethics Approval: I have followed the ethical principles and accurate references to scientific sources in my original article.

Consent to Participate: Informed consent was obtained from all authors.

Consent for Publication: I consent to the publication of my original research article.

References and Notes:

1. Bertoluzzi L, Ma S (2012) On the methods of calculation of the charge collection efficiency of dye sensitized solar cells. *Phys Chem Chem Phys* 15(12):4283–4285. <https://doi.org/10.1039/c3cp44248a>.
2. Gratzel M (2005) Solar Energy Conversion by Dye-Sensitized Photovoltaic Cells. *Inorg Chem* 44(20):6841–6851. <https://doi.org/10.1021/ic0508371>.
3. Katoh R, Furube A (2014) Electron injection efficiency in dye-sensitized solar cells. *J Photochem Photobiol C* 20:1–16. <https://doi.org/10.1016/j.jphotochemrev.2014.02.001>.
4. Liu M, Johnston M B., Snaith H J. (2013) Efficient planar heterojunction perovskite solar cells by vapour deposition. *Nature* 501(7467):395–398. <https://doi.org/10.1038/nature12509>.
5. Park N.-G (2015) Perovskite solar cells: an emerging photovoltaic technology. *Mater. Today* 18(2):65–72. <https://doi.org/10.1016/j.mattod.2014.07.007>.
6. Wu R, Yang Y, Li M, Qin D, Zhang Y, Hou L (2017) Solvent Engineering for High-Performance PbS Quantum Dots Solar Cells. *Nanomaterials* 7(8):201(1–13). <https://doi.org/10.3390/nano7080201>.
7. Wang Z, Hu Z, Kamarudin M A, Kapil G, Tripathi A, Shen Q, Yoshino K, Minemoto T, Pandey Sham S., Hayase S (2018) Enhancement of charge transport in quantum dots solar cells by *N*-butylamine-assisted sulfur-crosslinking of PbS quantum dots. *Solar Energy* 174:399–408. <https://doi.org/10.1016/j.solener.2018.09.026>.
8. Yu P, Zhu K, Norman A G., Ferrere S, Frank Arthur J., Nozik Arthur J. (2006) Nanocrystalline TiO₂ Solar Cells Sensitized with InAs Quantum Dots. *J Phys Chem B* 110(50):25451–25454. <https://doi.org/10.1021/jp064817b>.
9. Shrotriya V, Li G, Yao Y, Moriarty T, Emery K, Yang Y (2006) Accurate Measurement and Characterization of Organic Solar Cells. *Adv Funct Mater* 16(15):2016–2023. <https://doi.org/10.1002/adfm.200600489>.
10. Morel D L, Ghosh A K, Feng T, Stogryn E L, Purwin P E (1978) High efficiency organic solar cells. *Appl Phys Lett* 32(8):495–497. <https://doi.org/10.1063/1.90099>.
11. Stuart H R., Hall D G. (1996) Absorption enhancement in silicon on insulator waveguides using metal island films. *Appl Phys Lett* 69(16):2327–2339. <https://doi.org/10.1063/1.117513>.

12. Said D A, Ali A M, Khayyat M M, Boustimi M, Loulou M, Seoudi R (2019) A study of the influence of plasmonic resonance of gold nanoparticle doped PEDOT: PSS on the performance of organic solar cells based on CuPc/C6₀. *Heliyon* 5(11):e02675. <https://doi.org/10.1016/j.heliyon.2019.e02675>.
13. Notarianni M, Vernon K, Chou A, Aljada M, Liu J, Motta N (2014) Plasmonic effect of gold nanoparticles in organic solar cells. *Solar Energy* 106:23–37. <https://doi.org/10.1016/j.solener.2013.09.026>.
14. Su Y.-H, Ke Y.-F, Cai S.-L, Yao Q.-Y (2012) Surface plasmon resonance of layer-by-layer gold nanoparticles induced photoelectric current in environmentally-friendly plasmon-sensitized solar cell. *Light Sci Appl* 1(6):e14. <https://doi.org/10.1038/lsa.2012.14>.
15. Baryshnikova K V, Petrov M I, Babicheva V E, Belov P A (2016) Plasmonic and silicon spherical nanoparticle antireflective coatings. *Sci Rep* 6:22136(1–11). <https://doi.org/10.1038/srep22136>.
16. Lesina A C, Paternoster G, Mattedi F, Ferrario L, Berini P, Ramunno L, Paris A, Vaccari A, Calliari L (2015) Modeling and Characterization of Antireflection Coatings with Embedded Silver Nanoparticles for Silicon Solar Cells. *Plasmonics* 10(6):1525–1536. <https://doi.org/10.1007/s11468-015-9957-7>.
17. Singh H K, Sandeep K, Chary M, Balraj A, Sharma P, Solanki C S (2014) Investigation on silver nanoparticles-based plasmonic antireflection and its impact on electrical performance of mono c-Si solar cells. 2014 IEEE 2nd International Conference on Emerging Electronics (ICEE) 1–4. <https://doi.org/10.1109/ICEmElec.2014.7151167>.
18. Zhang Y, Cai B, Jia B (2016) Ultraviolet Plasmonic Aluminium Nanoparticles for Highly Efficient Light Incoupling on Silicon Solar Cells. *Nanomaterials* 6(6):95(1–10). <https://doi.org/10.3390/nano6060095>.
19. Parashar P K, Sharma R P, Komarala V K (2016) Plasmonic silicon solar cell comprised of aluminum nanoparticles: Effect of nanoparticles' self-limiting native oxide shell on optical and electrical properties. *J Appl Phys* 120(14):143104-1–143104-9. <https://doi.org/10.1063/1.4964869>.
20. Temple T L, Bagnall D M (2011) Optical properties of gold and aluminium nanoparticles for silicon solar cell applications. *J Appl Phys* 109(8):084343-1–084343-1. <https://doi.org/10.1063/1.3574657>.
21. Wu X, Liu P, Ma L, Zhou Q, Chen Y, Lu J, Yang S.-e (2016) Two-dimensional modelling of TiO₂ nanowire based organic–inorganic hybrid perovskite solar cells. *Sol Energy Mater Sol Cells* 152:111–117. <https://doi.org/10.1016/j.solmat.2016.03.017>.
22. Wang Y.-C, Chen C.-Y, Kuo C.-W, Kuan T.-M, Yu C.-Y, Chen I-C (2016) Low-temperature grown indium oxide nanowire-based antireflection coatings for multi-crystalline silicon solar cells. *Phys Status Solidi* 213(8):2259–2263. <https://doi.org/10.1002/pssa.201600005>.
23. Leem D.-S, Edwards A, Faist M, Nelson J, Bradley Donal D C, de Mello J C (2011) Efficient Organic Solar Cells with Solution-Processed Silver Nanowire Electrodes. *Adv Mater* 23(38):4371–4375. <https://doi.org/10.1002/adma.201100871>.
24. Parayil S K, Lee Y M, Yoon M (2009) Photoelectrochemical solar cell properties of heteropolytungstic acid-incorporated TiO₂ nanodisc thin films. *Electrochem commun* 11(6):1211–1216. <https://doi.org/10.1016/j.elecom.2009.04.031>.

25. Rockstuhl C, Lederer F (2009) Photon management by metallic nanodiscs in thin film solar cells. *Appl Phys Lett* 94(21):213102-1–213102-3. <https://doi.org/10.1063/1.3141402>.
26. Ali M, Zhou F, Chen K, Kotzur C, Xiao C, Bourgeois L, Zhang X, MacFarlane D R (2016) Nanostructured photoelectrochemical solar cell for nitrogen reduction using plasmon-enhanced black silicon. *Nat Commun* 7:11335(1–5). <https://doi.org/10.1038/ncomms11335>.
27. Luther J M, Law M, Beard M C, Song Q, Reese M O, Ellingson R J, Nozik A J (2008) Schottky Solar Cells Based on Colloidal Nanocrystal Films. *Nano Lett* 8(10):3488–3492. <https://doi.org/10.1021/nl802476m>.
28. Ergen O, Gibb A, Vazquez-Mena O, Regan W R, Zettl A (2015) Metal insulator semiconductor solar cell devices based on a Cu₂O substrate utilizing h-BN as an insulating and passivating layer. *Appl Phys Lett* 106(10):103904-1–103904-4. <https://doi.org/10.1063/1.4914181>.
29. Shewchun J, Burk D, Spitzer M B (1980) MIS and SIS Solar Cells. *IEEE Trans Electron Devices* 27(4):705–716.
30. Sarkar M B, Choudhuri B, Bhattacharya P, Barman R N, Ghosh A, Dwivedi S M M D, Chakrabarty S, Mondal A (2018) Improved UV Photodetection by Indium Doped TiO₂ Thin Film Based Photodetector. *J Nanosci Nanotechnol* 18(7):4898–4903. <https://doi.org/10.1166/jnn.2018.15295>.
31. Nath A, Sarkar M B (2021) Surface-Plasmon-Induced Ag Nanoparticles Decorated In₂O₃ Nanowires for Low Noise Photodetectors. *Plasmonics* 16(1):37–48. <https://doi.org/10.1007/s11468-020-01262-z>.
32. Nath A, Raman R, Singh L R, Sarkar M B (2021) Enhanced Photodetection in Glancing Angle Deposited One-Dimensional In₂O₃ Nanorod Array. *J Nanosci Nanotechnol* 21(5):3115–3122. <https://doi.org/10.1166/jnn.2021.19280>.
33. Anand K, Kaur J, Singh R C, Thangaraj R (2016) Structural, optical and gas sensing properties of pure and Mn-doped In₂O₃ nanoparticles. *Ceramics International* 42(9):10957–10966. <https://doi.org/10.1016/j.ceramint.2016.03.233>.
34. Dwivedi S M M D, Ghosh A, Deepthy S, Maji M, Lahiri R, Mondal S, Ghosh C, Dalal A, Mondal A, Ghosh M (2020) Detection technique for vitamin D₃ using Er-doped TiO₂ nanowire-based UV photodetector. *J Nanophoton* 14(4):046001-1–046001-17. <https://doi.org/10.1117/1.JNP.14.046001>.
35. Xie W, Li Y, Sun W, Huang J, Xie H, Zhao X (2010) Surface modification of ZnO with Ag improves its photocatalytic efficiency and photostability. *Journal of Photochemistry and Photobiology A: Chemistry* 216(2–3):149–155. <https://doi.org/10.1016/j.jphotochem.2010.06.032>.
36. Laskri A, Drici A, Boulouma A, Amara A, Bernede J C (2019) Investigation of Microstructural and Optical Properties of Ag₃O₄ Thin Films Sprayed onto Glass Substrate. *J Nano R* 58:90–101. <https://doi.org/10.4028/www.scientific.net/JNanoR.58.90>.
37. Nath A, Raman R, Yadav V K, Sannibabu P, Sarkar M B (2020) Bandgap Modulation of Glancing Angle Deposition Aided Ag Nanoparticles Covered TiO₂ Thin Film by High Temperature Annealing. *J Nanosci Nanotechnol* 20(12):7636–7643. <https://doi.org/10.1166/jnn.2020.18575>.
38. Kubelka P (1947) New Contributions to the Optics of Intensely Light-Scattering Materials. Part I. *J Opt Soc Am* 38(5):448–457. <https://doi.org/10.1364/JOSA.38.000448>.

39. Shin S G, Choi H W (2020) Improvement of Characteristics of Metal Doped TiO₂ Thin Film and Application to Perovskite Solar Cell. *J Nanosci Nanotechnol* 20(11):7130–7134. <https://doi.org/10.1166/jnn.2020.18846>.
40. Nath A, Mahajan B K, Singh L R, Vishwas S, Nanda R K, Sarkar M B (2021) Enhancing Detectivity of Indium-Oxide-Based Photodetectors via Vertical Nanostructuring Through Glancing Angle Deposition. *J Electron Mater* 1–9. <https://doi.org/10.1007/s11664-021-08889-6>.
41. Hassanien A S, Akl A A (2015) Influence of composition on optical and dispersion parameters of thermally evaporated non-crystalline Cd₅₀S_{50-x}Se_x thin films. *J Alloys Compd* 648:280–290. <https://doi.org/10.1016/j.jallcom.2015.06.231>.
42. Chantana J, Nishimura, Kawano Y, Teraji S, Watanabe T, Minemoto T (2019) Examination of relationship between Urbach energy and open-circuit voltage deficit of flexible Cu(In,Ga)Se solar cell for its improved photovoltaic performance. *ACS Appl Energy Mater* 2(11):7843–7849. <https://doi.org/10.1021/acsaem.9b01271>.
43. Chen Y, Xu X L, Zhang G H, Xue H, Ma S Y (2009) A comparative study of the microstructures and optical properties of Cu- and Ag-doped ZnO thin films. *Physica B* 404(20):3645–3649. <https://doi.org/10.1016/j.physb.2009.06.051>.
44. Zhao H, Huang F, Hou J, Liu Z, Wu Q, Cao H.-bin, Jing Q, Peng S, Cao G (2016) Efficiency enhancement of quantum dot sensitized TiO₂/ZnO nanorod arrays solar cells by plasmonic Ag nanoparticles. *ACS Appl Mater Interfaces* 8(40):26675–26682. <https://doi.org/10.1021/acsami.6b06386>.
45. Tachibana Y, Hara K, Sayama K, Arakawa H (2002) Quantitative Analysis of Light-Harvesting Efficiency and Electron-Transfer Yield in Ruthenium-Dye-Sensitized Nanocrystalline TiO₂ Solar Cells. *Chem Mater* 14(6):2527–2535. <https://doi.org/10.1021/cm011563s>.
46. Saravanan S, Kato R, Balamurugan M, Kaushik S, Soga T (2017) Efficiency improvement in dye sensitized solar cells by the plasmonic effect of green synthesized silver nanoparticles. *Journal of Science: Advanced Materials and Devices* 2(4):418–424. <https://doi.org/10.1016/j.jsamd.2017.10.004>.
47. Wang Z.-S, Kawauchi H, Kashima T, Arakawa H (2004) Significant influence of TiO₂ photoelectrode morphology on the energy conversion efficiency of N719 dye-sensitized solar cell. *Coordination Chemistry Reviews* 248(13–14):1381–1389. <https://doi.org/10.1016/j.ccr.2004.03.006>.
48. Ogawa Y, Jäger-Waldau A, Hashimoto Y, Ito K (1994) In₂O₃/CdS/CuInS₂ Thin-Film Solar Cell with 9.7% Efficiency. *Jpn J Appl Phys* 33(Part 2, No. 12B):L1775–L1777. <https://doi.org/10.1143/JJAP.33.L1775>.
49. Sharma J R, Das G, Roy A B, Bose S, Mukhopadhyay S (2020) Design Analysis of Heterojunction Solar Cells with Aligned AZO Nanorods Embedded in p-type Si wafer. *Silicon* 12(2):305–316. <https://doi.org/10.1007/s12633-019-00134-4>.
50. Hara K, Sayama K, Ohga Y, Shinpo A, Suga S, Arakawa H (2001) A coumarin-derivative dye sensitized nanocrystalline TiO₂ solar cell having a high solar-energy conversion efficiency up to 5.6%. *Silicon* 6:569–570. <https://doi.org/10.1039/b010058g>.
51. Kim D H, Lee S, Park J H, Noh J H, Park I J, Seong W M, Hong K S (2011) Transmittance optimized nb-doped TiO₂/Sn-doped In₂O₃ multilayered photoelectrodes for dye-sensitized solar cells. *Solar Energy Materials and Solar Cells* 96:276–280. <https://doi.org/10.1016/j.solmat.2011.09.011>.

52. Shen T, Tian J, Lv L, Fei C, Wang Y, Pullerits T, Cao G (2016) Investigation of the role of Mn dopant in CdS quantum dot sensitized solar cell. *Electrochim Acta* 191:62–69. <https://doi.org/10.1016/j.electacta.2016.01.056>.
53. Saha S, Das P, Chakraborty A K, Sarkar S, Debbarma R (2016) Fabrication of DSSC with Nanoporous TiO₂ Film and Kenaf Hibiscus Dye as Sensitizer. *Int J Renew Energy Res* 6(2):1–8.
54. Basu K, Benetti D, Zhao H, Jin L, Vetrone F, Vomiero A, Rosei F (2016) Enhanced photovoltaic properties in dye sensitized solar cells by surface treatment of SnO₂ photoanodes. *Sci Rep* 6(1):23312(1–10). <https://doi.org/10.1038/srep23312>.
55. Shashanka R, Esgin H, Yilmaz V M, Caglar Y (2020) Fabrication and characterization of green synthesized ZnO nanoparticle based dye-sensitized solar cells. *Journal of Science: Advanced Materials and Devices* 5(2):185–191. <https://doi.org/10.1016/j.jsamd.2020.04.005>.

Figures

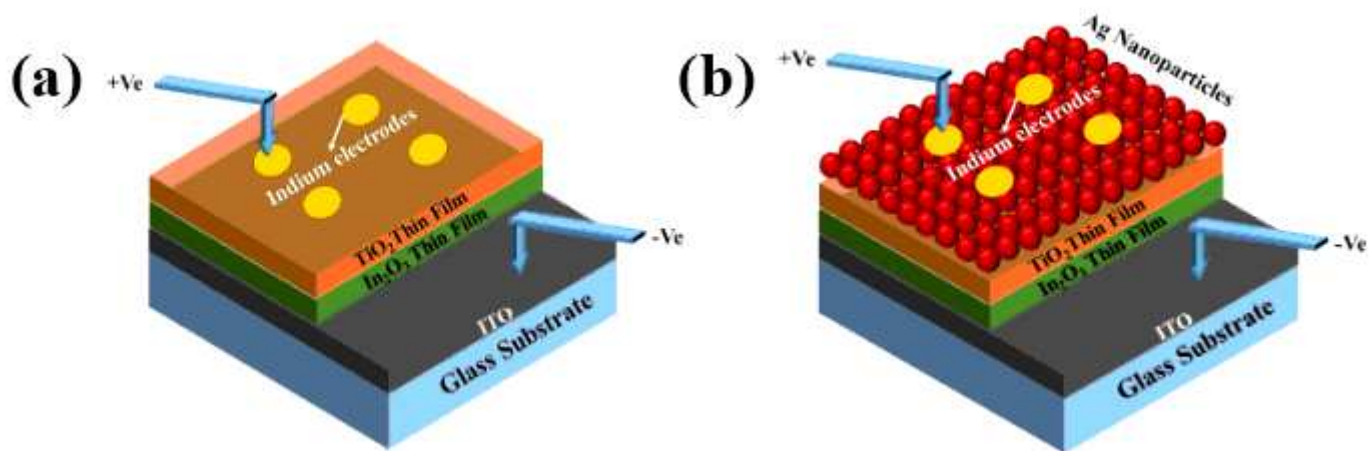


Figure 1

Schematic diagram of the fabricated devices: (a) In₂O₃/TiO₂ thin film, (b) In₂O₃/TiO₂ thin film/Ag nanoparticles.

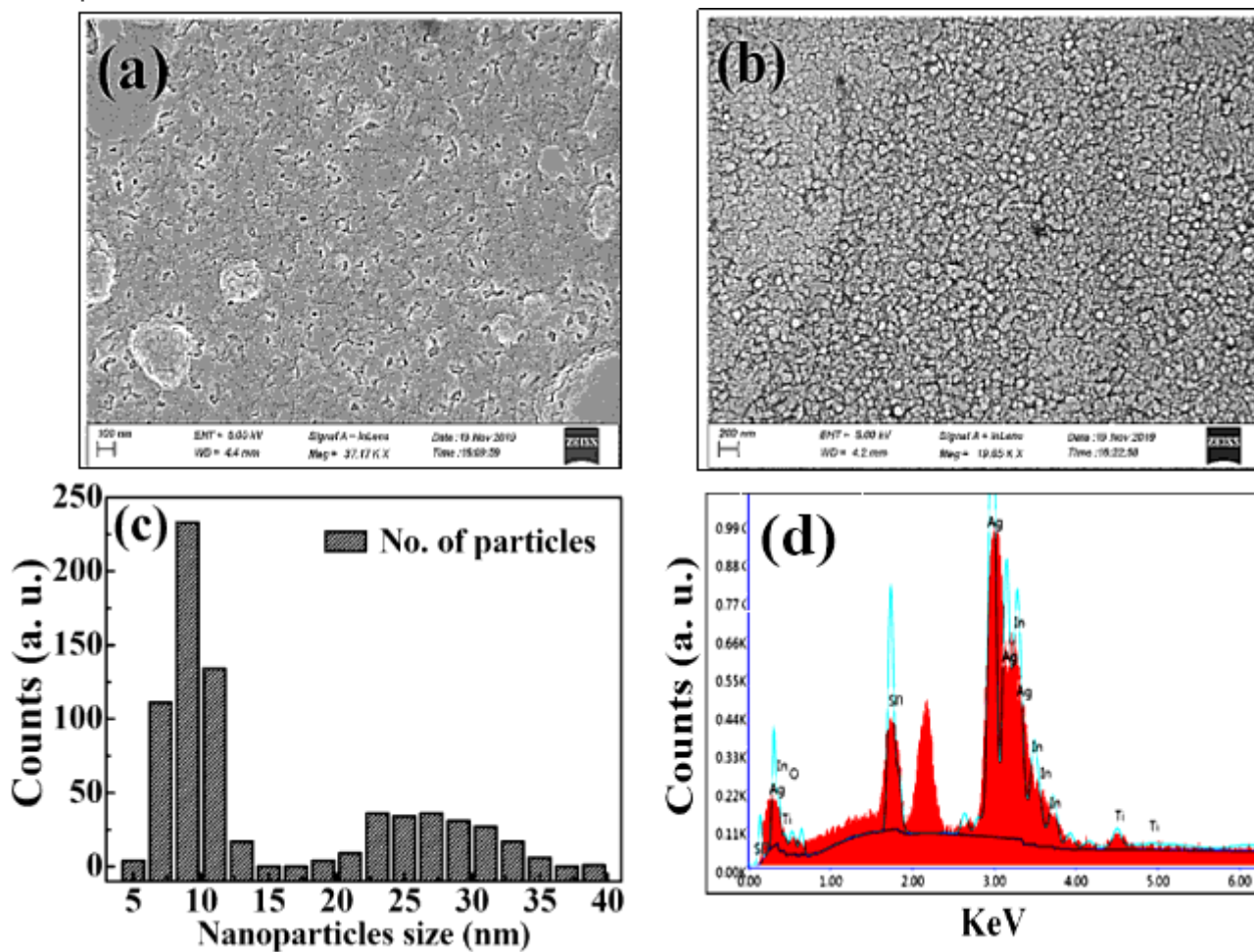


Figure 2

Top view FESEM images of (a) In₂O₃/TiO₂ thin film, (b) In₂O₃/TiO₂ thin film/Ag nanoparticles, (c) Particle size histogram image of Ag nanoparticles, (d) EDAX analysis of the sample.

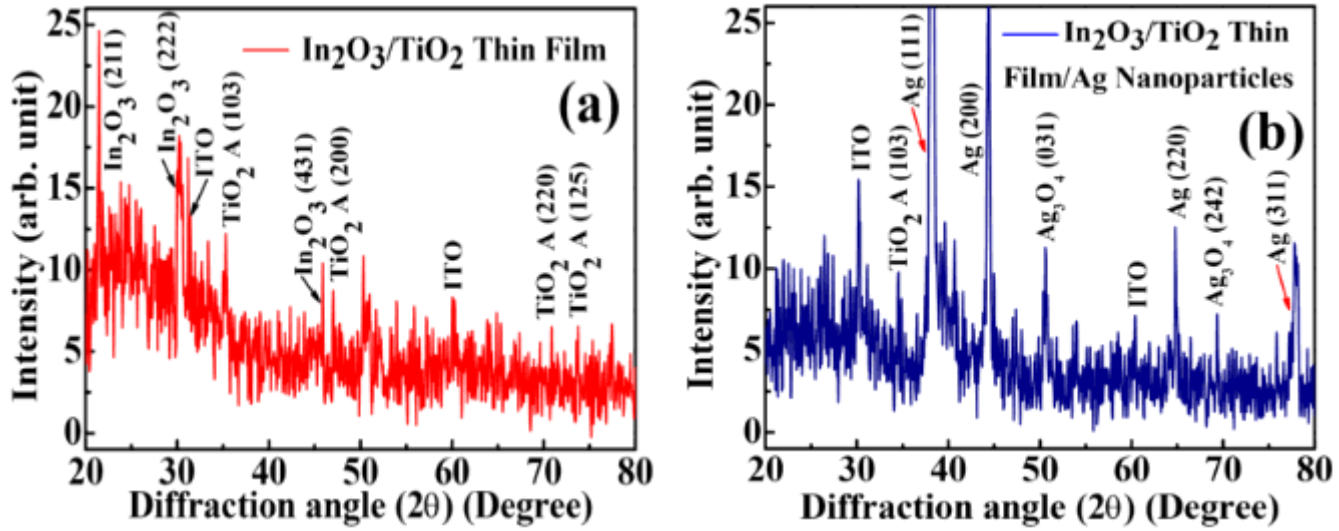


Figure 3

XRD profiles for (a) In₂O₃/TiO₂ thin film (b) In₂O₃/TiO₂ thin film/Ag nanoparticles.

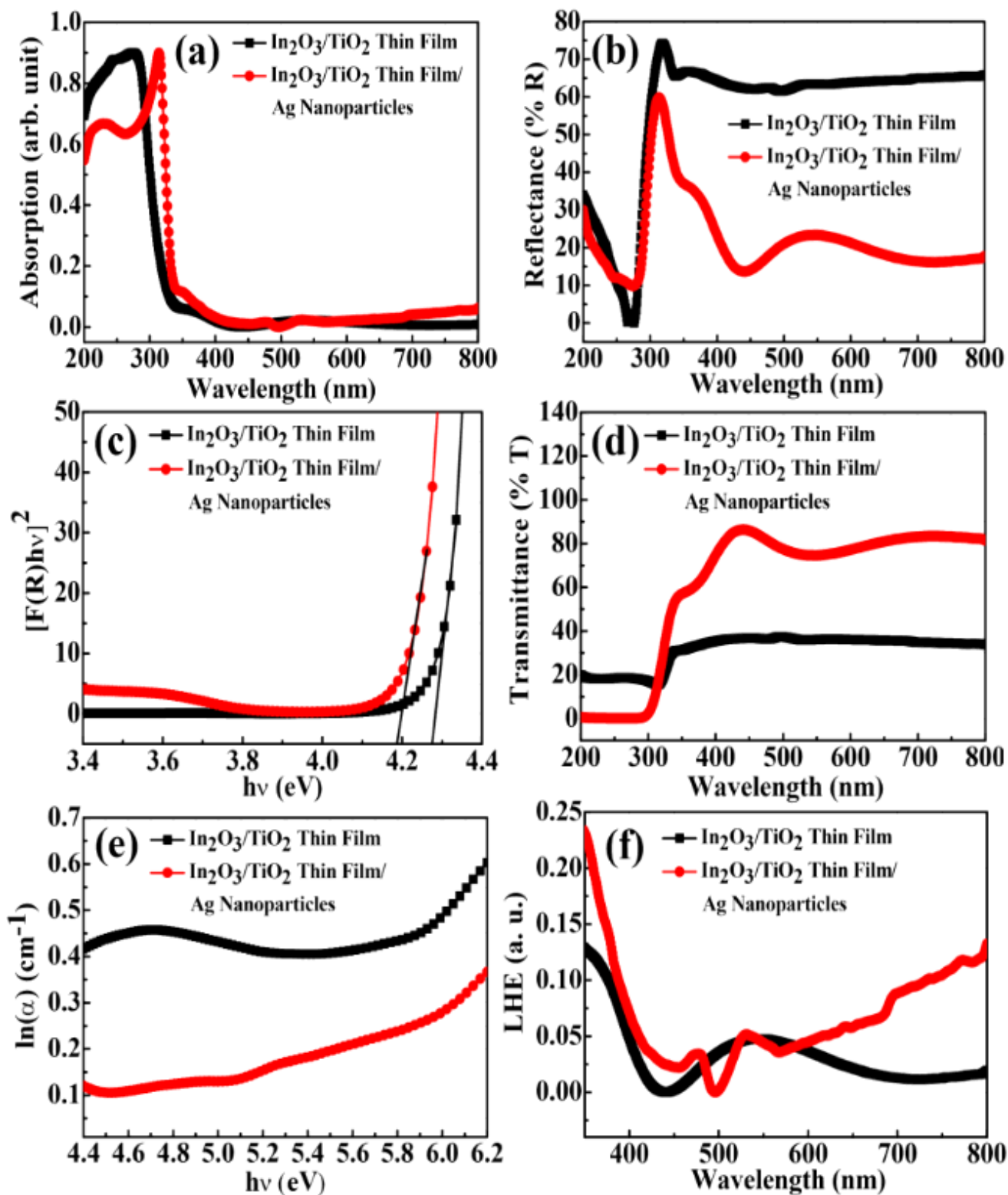


Figure 4

(a) Absorption spectra, (b) UV-DRS spectra (reflectance spectra), (c) Kubelka-Munk plot (for bandgap), (d) Transmittance spectra, (e) Urbach energy, (f) Light harvesting efficiency (LHE) characteristics of In₂O₃/TiO₂ thin film and In₂O₃/TiO₂ thin film/Ag nanoparticles samples on a ITO coated glass substrate.

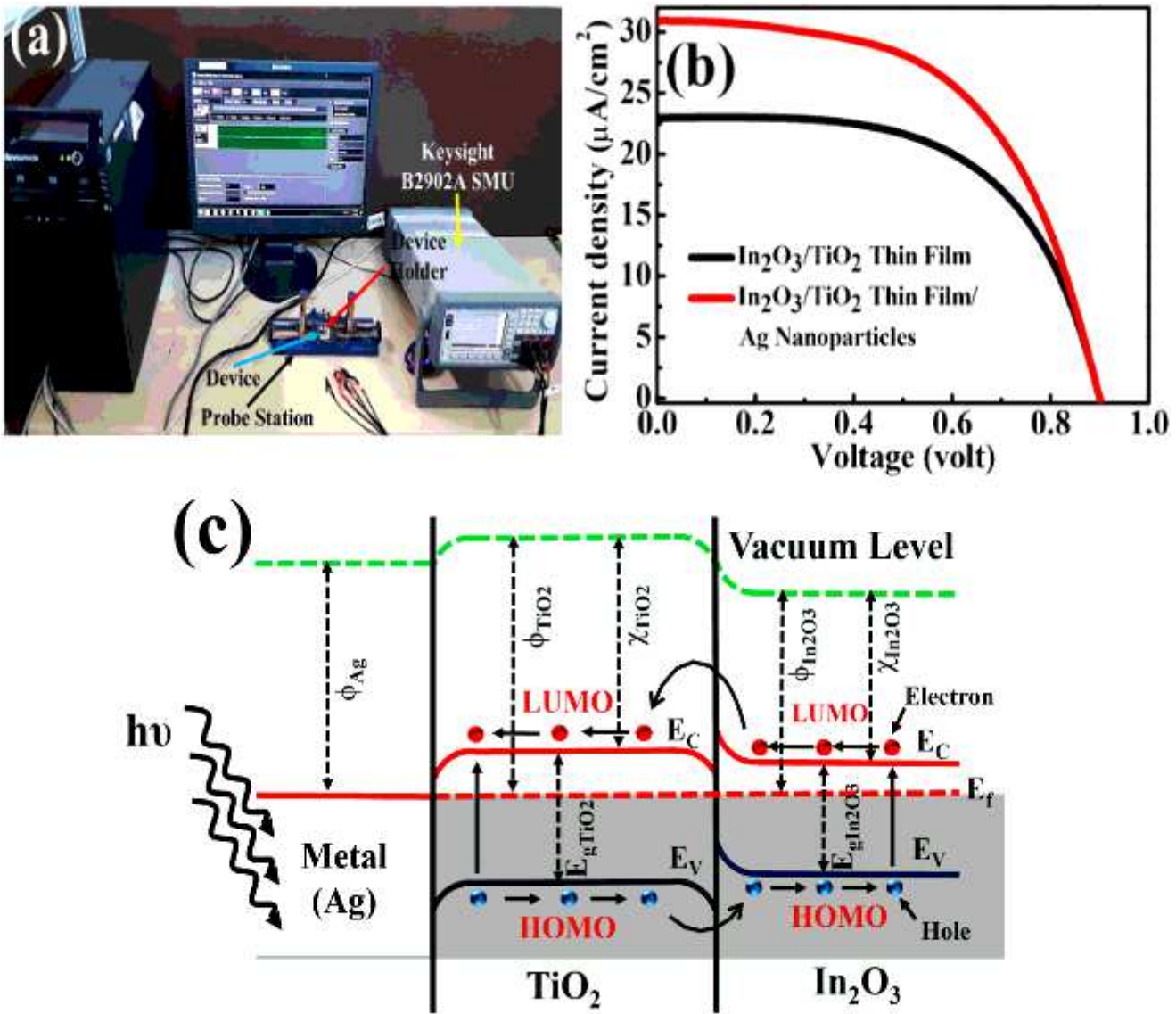


Figure 5

5 (a) Experimental setup for the measurement of photovoltaic parameters, (b) J-V curve for $\text{In}_2\text{O}_3/\text{TiO}_2$ thin film and $\text{In}_2\text{O}_3/\text{TiO}_2$ thin film/Ag nanoparticles devices, (c) A schematic illustration of the staggered gap diagram.